ChemComm

COMMUNICATION

View Article Online
View Journal | View Issue

Check for updates

Cite this: *Chem. Commun.*, 2020, **56**, 9994

Received 24th June 2020,
Accepted 21st July 2020

DOI: 10.1039/d0cc04400h

rsc.li/chemcomm

Published on 22 July 2020. Downloaded by University of Texas Libraries on 9/3/2020 9:55:04 PM.

Amethyrin-type expanded porphyrins that display anti-aromatic character upon protonation†

Harrison D. Root, ‡ Daniel N. Mangel, ‡ James T. Brewster II, ‡ Hadiqa Zafar, Adam Samia, Graeme Henkelman * and Jonathan L. Sessler *

The use of protonation to switch nonaromatic expanded porphyrins to their corresponding anti-aromatic forms has not been widely explored. Here, we show that free-base pyriamethyrin and dipyriamethyrin display nonaromatic character, as inferred from NMR spectroscopic analyses, their optical properties, and theoretical calculations. Addition of two protons extends the π – conjugation of these amethyrin analogues and yields formally anti-aromatic systems.

Aromaticity remains one of the most fundamental concepts in organic chemistry. Understanding the relationship between aromatic, non-aromatic, and anti-aromatic states is thus of widespread interest, as are mechanisms that can allow switching between these various limiting electronic forms. Playing a central role in these efforts are porphyrins and their analogues (collectively "porphyrinoids"). These macrocycles have proven indispensable in the context of biomedical studies, as well as material applications.[1–3] Expanded porphyrins are a particularly interesting class of porphyrinoids that have played a key role in advancing our understanding of aromaticity due to their ability to adopt a wide range of conformations and oxidation states.[4] Large expanded porphyrins have previously been used to access various aromatic and anti-aromatic forms, including twisted Hückel and Möbius aromatic species.[5,6] Metalation and proton coupled electron transfer have also been used to control the electronic states of expanded porphyrins. Much less explored is the effect of simple protonation to achieve switching between non-, anti-, and aromatic forms. However, so-called pyriporphyrin derivatives have shown the ability to switch between nonaromatic and aromatic forms upon protonation.[7,8] Additionally, some years ago we showed that cyclo[2]pyridine[4]pyrrole could be converted from its neutral non-aromatic form to the corresponding anti-aromatic species by means of diprotonation.[9] However, to our knowledge these findings have yet to be generalized. Here we report that pyriamethyrin (**1**) and dipyriamethyrin (**3**, **4**), analogues of amethyrin (**2**) (Fig. 1), are readily converted to anti-aromatic species upon protonation with methane sulfonic acid. We have also found that the inherent anti-aromaticity of **2** is increased upon protonation.

Amethyrin and its analogues (Fig. 1) have historically been of interest due to their coordination chemistry, as well as their ability to switch between various oxidation states upon metalation.[10–16] Recent work has brought to light how the inherent properties of this framework can be modified by introducing pyridine moieties into the terpyrrolic subunit.[17] This appreciation builds off of previous studies that implicate the pyridine unit as playing a key role in mediating the metal coordination chemistry relative to the parent hexapyrrolic species.[18–21] An open question was thus whether protonation could serve to endow amethyrin and its pyridine-containing analogues with additional conjugation pathways extending over the entirety of the periphery, thereby "opening up" global (anti)aromaticity for the system as a whole.[9,22] As detailed below we have now found that several pyridine-containing macrocycles, namely the asymmetric amethyrin (pyriamethyrin **1**) and two dipyriamethyrins (**3** and **4**), can be converted to the corresponding formal anti-aromatic forms by means of simple diprotonation (*cf. e.g.*, Fig. 2). Similar, but not identical effects, are seen in the case of amethyrin **2**.

Initial UV-Vis spectroscopic studies of **1** (Fig. 3) revealed a spectrum reminiscent of other amethyrin macrocycles with a

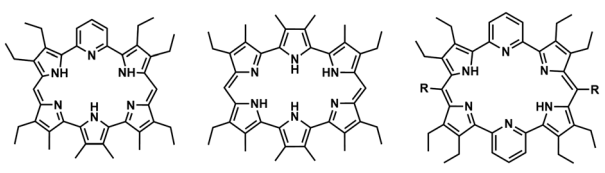

Fig. 1 Chemical structures of pyriamethyrin (**1**), amethyrin (**2**), and the dipyriamethyrins (**3** and **4**) considered in the present study.

Department of Chemistry, The University of Texas at Austin, 105 East 24th St., Stop A5300, Austin, USA. E-mail: sessler@cm.utexas.edu, henkelman@utexas.edu

† Electronic supplementary information (ESI) available. See DOI: 10.1039/d0cc04400h

‡ These authors contributed equally.

This journal is © The Royal Society of Chemistry 2020

Published on 22 July 2020. Downloaded by University of Texas Libraries on 9/3/2020 9:55:04 PM.

Fig. 2 Addition of 2 equivalents of methane sulfonic acid (MSA) yields the diprotonated anti-aromatic species **1b**.

strong Soret-like band at 452 nm (ε = 43 162 M^{-1} cm^{-1}) and two N-like bands at 373 nm and 285 nm (ε = 16 721 M^{-1} cm^{-1} and ε = 13 205 M^{-1} cm^{-1}, respectively). Evidence that protonation leads to π-conjugation that extends throughout the macrocycle came from a UV-Vis spectroscopic titration of **1** with methane sulfonic acid (MSA) (Fig. 3). Upon the addition of increasing quantities of MSA, a visible colour change from yellow to orange-red was observed. This colour change is accompanied by a red shift and an increase in the intensity of the Soret-like band (452 → 490 nm). A growing in of new N-type absorption features at 300 nm and 410 nm, as well as a Q-type band at 577 nm, is also seen. These spectral changes are rationalized in terms of forming the diprotonated species **1b** (Fig. 2).

Macrocycles **2** and **3** also showed changes in their UV-Vis spectral features upon exposure to MSA. Upon titration with MSA, solutions of **2** in $CHCl_3$ a dramatic increase in the intensity of the Soret-like band at 488 nm is seen, along with the appearance of a new Q-type band at 591 nm (ESI,† Fig. S1). The UV-Vis spectrum of macrocycle **4** revealed a red shift and an increase in the intensity of the Soret-like band (470 nm → 516 nm), as well as the growing in of an N-type feature at 381 nm. Additionally, Q-type bands are seen at 592 nm and 646 nm upon treatment with MSA (ESI,† Fig. S2). Again, these spectral changes were attributed to the formation of the diprotonated form of **4** and interpreted in terms of an effective expansion of the π-conjugation

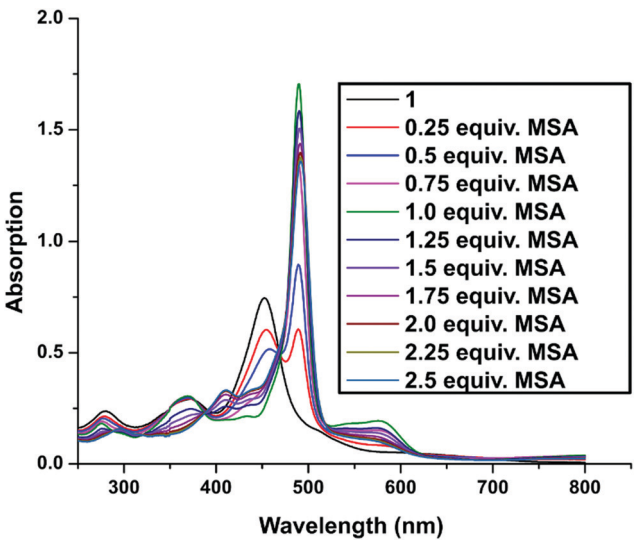

Fig. 3 UV-Vis spectral titration of **1** with MSA in $CHCl_3$. The red shift in the Soret-like band and the appearance of Q-type features was taken as initial evidence of extended π-conjugation.

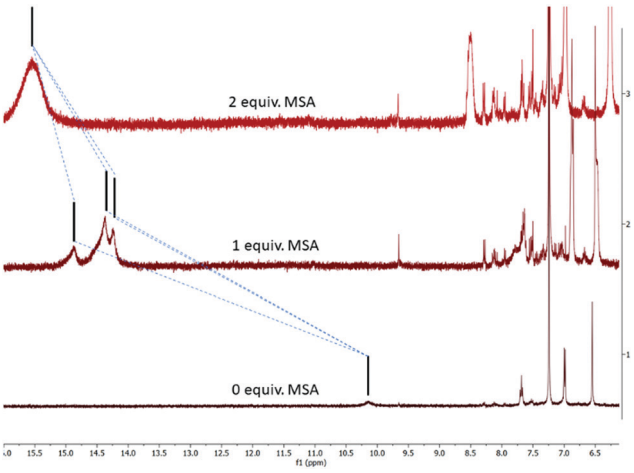

Fig. 4 NMR spectral titration of **1** in $CDCl_3$ with MSA-d_4. The downfield shift in the pyrrole N*H* resonance seen upon diprotonation is taken as evidence for conversion to an antiaromatic form.

pathways present within this and the other amethyrin-type macrocycles considered in this study.

Further support for a proton-coupled expansion of the π-conjugation periphery came from ^{1}H NMR spectral studies. The free-base form of pyriamethyrin **1** in $CDCl_3$ displays pyrrole N*H* resonances that match those seen for a number of other nonaromatic porphyrinoid cores (*i.e.*, δ = 10.14 ppm, Fig. 4). In contrast, upon addition of two equivalents of MSA-d_4, these signals shift downfield to 15.5 ppm, indicating a more strongly deshielded environment. Intermediate shift behaviour is seen upon addition of only 1 equivalent of MSA with a splitting of the pyrrole N*H* resonances also being observed. This latter splitting is likely due to the asymmetry of the pyrrole N*H* protons that is induced upon addition of only one equivalent of MSA to **1**. However, once two equivalents of MSA are added (forming diprotonated **1b**) the N*H* resonances coalesce back to a single peak. This could reflect a fast exchange process or regeneration of a symmetric structure. We consider the latter explanation more likely. The downfield shift of the pyrrole N*H* resonances is consistent with the presence of an anti-aromatic paratropic ring current wherein the protons within the ring exist in a less shielded environment and therefore experience a downfield shift in the ^{1}H NMR spectrum.

The free-base form of amethyrin **2** displayed pyrrole N*H* resonances (12.10 ppm and 12.82 ppm) that are similar to what is seen in the case of **1**. Upon protonation, these pyrrole *N*H signals shift far downfield to 19.9 ppm (ESI,† Fig. S3). Again, this was taken as evidence that the diprotonated form of **2** displays anti-aromatic character. As true for **1**, the addition of 1 equivalent of MSA to **3** gives rise to splitting in this signal that coalescences back to a singlet upon the addition of 2 equivalents; however, the spectra is more convoluted, making discrimination between discrete protonation states difficult. Dipyriamethyrin **3** displays the same trend as observed for **1** and **2** (ESI,† Fig. S4). The pyrrole N*H* resonances of the neutral form appear at 6.91 ppm (a chemical shift typical for non-aromatic systems). As above, the addition of 1 equivalent of MSA causes the N*H* resonances to split into several

Published on 22 July 2020. Downloaded by University of Texas Libraries on 9/3/2020 9:55:04 PM.

broad peaks that coalesce to two sharp peaks at 11.25 ppm and 10.83 ppm, respectively, upon the addition of two equivalents of MSA. These findings are again attributed to the asymmetry induced by the addition of one proton and symmetry being restored once two protons are added to the macrocycle.

To obtain further insight into the electronic nature of these amethyrin species, density functional theory (DFT) calculations were carried out using the Gaussian 16 package and the Stampede2 cluster at the Texas Advanced Computational Center (TACC) and the Halifax server at the Oden Institute for Computational Engineering and Sciences.[23,24] Geometric relaxations were carried out using X-ray crystal structural parameters for freebase compounds **1–4** so as to obtain energy minimized structures and simulated spectra.[8,9,13] Agreement between experimental and theoretical data was seen in all cases.

Aromaticity was evaluated using several well-known methods. First, gauge including magnetic induced current (GIMIC) density calculations were performed on the series of expanded porphyrins.[25–30] Integrated current densities were evaluated and the main current pathways densities for selected bonds were determined (ESI,† Fig. S5). In all cases protonation induced a significant change in the current pathways. Both free-base complexes **1** and **3** displayed a minor paratropic current throughout the macrocycle, indicating that these free-base ligands experience no significant global conjugation. Furthermore, these free-base complexes displayed a high degree of local aromaticity, as observed by strong diatropic ring currents within the pyrrole and pyridine subunits. Diprotonation of complexes **1** and **3** resulted in reduction of the local aromaticity present within the pyridine and pyrrole sub-units as observed by a decrease in the current density. Loss of local aromaticity was accompanied by a gain of a global paratropic current, indicating a newly formed anti-aromatic pathway. Interestingly, in contrast to complexes **1** and **3**, free-base amethyrin **2** is characterized by a significant global paratropic current. This observation supports prior reports wherein the free-base form of amethyrin is formally antiaromatic.[31] In analogy to what is true for **1** and **3**, protonation of **2** results in a significant increase in the global paratropic current that involves an outer conjugative pathway through the pyrrolic subunits. This increase comes at the cost of near-complete loss in local aromaticity.

Anisotropy of the induced current density (ACID) calculations provide further support for the conclusion that expanded porphyrins **1–4** display proton induced anti-aromaticity.[32] For the protonated species, the ACID plots calculated with the applied magnetic field along the *z*-axis, show a strong dominant paratropic ring current in all cases, indicative of an anti-aromatic pathway (Fig. 5).

In contrast, the free base forms **1** and **3** displayed little global current directionality. Rather, strong diatropic currents were seen within the local aromatic subunits. This local aromaticity is disrupted upon protonation as reflected in a reduction in the local diatropic ring currents. However, it translates directly into a net increase in global conjugation. The calculated magnetic current density data is in agreement

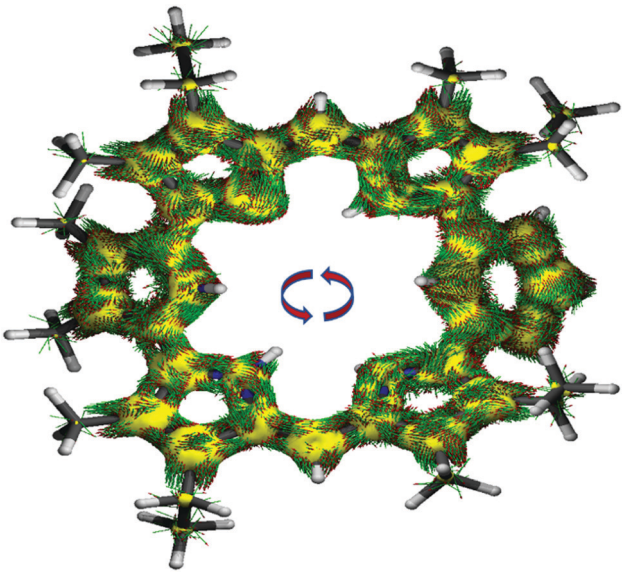

Fig. 5 Calculated anisotropy induced current density (ACID) plot for diprotonated pyriamethyrin **1b**. Current density vectors associated with a global counter-clockwise current are seen, as would be expected for an anti-aromatic compound.

with the experimental ^{1}H NMR spectral studies (Fig. 4) where the observed downfield shifts in the inner N*H* proton signals are ascribed to the presence of an inner paratropic ring current that serves to deshield the N*H* proton (ESI,† Fig. S9–S20).

Nucleus independent chemical shifts (NICS) were calculated at the center of the macrocycle, as defined by the centroid of the six nitrogen atoms, located 1 Å above the center. In all cases, significant differences in the NICS$(1)_{zz}$ values between the free-base and protonated forms were observed.[33] The NICS$(1)_{zz}$ values for the free-base forms of **1** and **3** were 4.68 and 3.23 ppm, respectively. While the NICS values of these metal-free porphynoids are characterized by slight paratropic current, free-base amethyrin **2** displayed a large positive NICS$(1)_{zz}$ value of 20.42 ppm. This result is consistent with free-base amethyrin being an anti-aromatic compound as noted earlier.[31] Upon protonation of the free-base forms of **1** and **3**, a significant shift in the NICS$(1)_{zz}$ values to 16.6 and 28.2 ppm, respectively, was observed. Likewise, diprotonation of amethyrin **2b** led to a drastic shift in the NICS$(1)_{zz}$ value to 43.2 ppm. The isochemical surface shielding (ICSS) plot, for ligands **1** and **3**, are shown in Fig. 6. It is noteworthy that amethyrins **2** and **2b** displayed the highest anti-aromatic character, followed by pyriamethyrin **1b** and dipyriamethyrin **3b**. On this basis, we suggest that substitution of pyrrole with pyridine in the case of the amethyrin class of expanded porphyrins results in reduced through-conjugation and global anti-aromaticity. This conclusion is consistent with the differences in the chemical shift changes in the pyrrole N*H* resonances due to protonation seen in the NMR titration experiments discussed above.

Upon protonation, the energy gaps between the HOMO and LUMO in **1b–3b** are reduced as compared to those of the corresponding neutral forms **1–3**. The lowering of the HOMO–LUMO gap is consistent with the idea that protonation induces anti-aromaticity.

 This journal is © The Royal Society of Chemistry 2020

Published on 22 July 2020. Downloaded by University of Texas Libraries on 9/3/2020 9:55:04 PM.

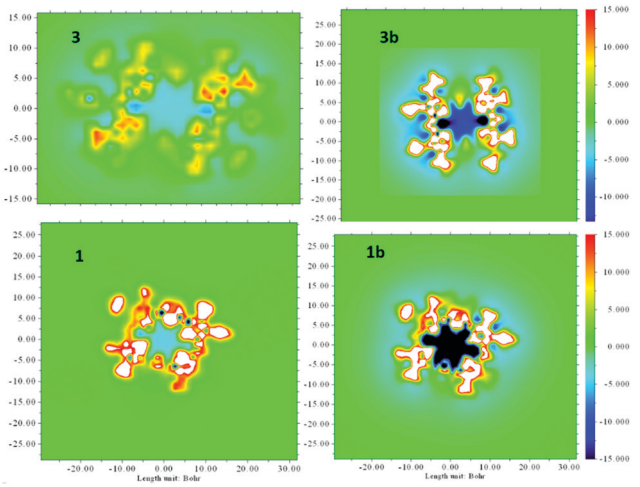

Fig. 6 Iso-chemical surface shielding (ICSS) of pyriamethyrin **1** and **3** dipyriamethyrin and their protonated forms. Green regions indicate non-aromatic, blue-black indicate antiaromaticity, and red indicates aromaticity.

A trend is also observed where the HOMO–LUMO gap increases upon replacing pyrrole with pyridine. The HOMO–LUMO gap for dipyriamethyrin complex **3** is 2.8 eV, while that for **2** is 2.0. This is consistent with the conclusion that the free-base macrocycle **2** already displays anti-aromatic character. However, upon protonation the HOMO–LUMO gap for complex **2b** decreases to 1.6 eV, supporting the notion that the anti-aromaticity is further increased upon protonation.

DFT calculations were performed on both the free-base and protonated forms of **1–3**. Based on these results we suggest that in all cases an increase in anti-aromatic character results from protonation. This increase in anti-aromatic character is accompanied by a significant reduction in local aromaticity in the case of **1b** and **3b**, and a complete loss of local aromaticity in the case of **2b**.

In summary, this study provides a set of rare examples in porphyrinoid chemistry where a conversion to an anti-aromatic form occurs as the result of simple protonation.

This work was supported by the Office of Basic Energy Sciences, U.S. Department of Energy (DOE) (Grant DEFG02-01ER15186 to J. L. S.), and the Robert A. Welch Foundation (F-1018 to J. L. S.). The authors acknowledge the Texas Advanced Computer Center (TACC) at The University of Texas at Austin for providing high performance computing resources that have contributed to the research results reported in this paper. H. D. R. thanks UT Austin for a Provost's Graduate Excellence Fellowship and the Environmental Institute at The University of Texas at Austin for a Scientist in Residence Fellowship. D. N. M. thanks UT Austin for the Graduate Research Fellowship. We thank the Laboratory Directed Research and Development (LDRD) program for a Glenn T. Seaborg Graduate Summer Student Fellowship (J. T. B.).

Conflicts of interest

There are no conflicts to declare.

Notes and references

1 L. P. Cook, G. Brewer and W. Wong-Ng, *Crystals*, 2017, **7**, 223.
2 M. Imran, M. Ramzan, A. K. Qureshi, M. Azhar Khan and M. Tariq, *Biosensors*, 2018, **8**, 1–17.
3 H. Huang, W. Song, J. Rieffel and J. F. Lovell, *Front. Phys.*, 2015, **3**, 1–15.
4 A. Osuka and S. Saito, *Chem. Commun.*, 2011, **47**, 4330–4339.
5 T. Soya, H. Mori and A. Osuka, *Angew. Chem., Int. Ed.*, 2018, **57**, 15882–15886.
6 Z. S. Yoon, A. Osuka and D. Kim, *Nat. Chem.*, 2009, **1**, 113–122.
7 R. Myśliborski, L. Latos-Grazyński and L. Szterenberg, *Eur. J. Org. Chem.*, 2006, 3064–3068.
8 T. D. Lash, K. Pokharel, J. M. Serling, V. R. Yant and G. M. Ferrence, *Org. Lett.*, 2007, **9**, 2863–2866.
9 Z. Zhang, J. M. Lim, M. Ishida, V. V. Roznyatovskiy, V. M. Lynch, H. Y. Gong, X. Yang, D. Kim and J. L. Sessler, *J. Am. Chem. Soc.*, 2012, **134**, 4076–4079.
10 R. J. P. Corriu, G. Bolin, J. J. E. Moreau and C. Vernhet, *J. Chem. Soc., Chem. Commun.*, 1991, 211–213.
11 F. H. Carré, R. J. P. Corriu, G. Bolin, J. J. E. Moreau and C. Vernhet, *Organometallics*, 1993, **12**, 2478–2486.
12 S. Hannah, D. Seidel, J. L. Sessler and V. Lynch, *Inorg. Chim. Acta*, 2001, **317**, 211–217.
13 J. T. Brewster, H. D. Root, D. Mangel, A. Samia, H. Zafar, A. C. Sedgwick, V. M. Lynch and J. L. Sessler, *Chem. Sci.*, 2019, 5596–5602.
14 E. Steiner and P. W. Fowler, *Org. Biomol. Chem.*, 2006, **4**, 2473–2476.
15 J. L. Sessler, A. Gebauer, A. Guba, M. Scherer and V. Lynch, *Inorg. Chem.*, 2002, **37**, 2073–2076.
16 J. T. Brewster, A. Aguilar, G. Anguera, H. Zafar, M. D. Moore and J. L. Sessler, *J. Coord. Chem.*, 2018, **71**, 1808–1813.
17 J. T. Brewster, Q. He, G. Anguera, M. D. Moore, X. S. Ke, V. M. Lynch and J. L. Sessler, *Chem. Commun.*, 2017, **53**, 4981–4984.
18 S. Durot, J. Taesch and V. Heitz, *Chem. Rev.*, 2014, **114**, 8542–8578.
19 Z. Zhou and Z. Shen, *J. Mater. Chem. C*, 2015, **3**, 3239–3251.
20 Y. Liu, Q. Zhang, Q. H. Guo and M. X. Wang, *J. Org. Chem.*, 2016, **81**, 10404–10410.
21 Z. Zhang, D. S. Kim, C. Y. Lin, H. Zhang, A. D. Lammer, V. M. Lynch, I. Popov, O. S. Miljanić, E. V. Anslyn and J. L. Sessler, *J. Am. Chem. Soc.*, 2015, **137**, 7769–7774.
22 R. R. Valiev, I. Benkyi, Y. V. Konyshev, H. Fliegl and D. Sundholm, *J. Phys. Chem. A*, 2018, **122**, 4756–4767.
23 M. J. Frisch, *et al.*, *Gaussian 16, Revision B.01*, Gaussian Inc., Wallingford, 2016.
24 Texas Advanced Computing Center (TACC), The University of Texas at Austin.
25 J. Juselius, D. Sundholm and J. Gauss, *J. Chem. Phys.*, 2004, **121**, 3952–3963.
26 H. Fliegl, S. Taubert, O. Lehtonen and D. Sundholm, *Phys. Chem. Chem. Phys.*, 2011, **13**, 20500–20518.
27 H. Fliegl, J. Jusélius and D. Sundholm, *J. Phys. Chem. A*, 2016, **120**, 5658–5664.
28 M. Rauhalahti, S. Taubert, D. Sundholm and V. Liegeois, *Phys. Chem. Chem. Phys.*, 2017, **19**, 7124–7131.
29 H. Fliegl, D. Sundholm, S. Taubert, J. Jusélius and W. Klopper, *J. Phys. Chem. A*, 2009, **113**(30), 8668–8676.
30 H. Fliegl, R. Valiev, F. Pichierri and D. Sundholm, *Chem. Modell.*, 2018, **14**, 1.
31 E. Steiner and P. W. Fowler, *Org. Biomol. Chem.*, 2006, **4**, 2473–2476.
32 R. Herges and D. Geuenich, *J. Phys. Chem. A*, 2001, **105**, 3214–3220.
33 Z. Chen, C. S. Wannere, C. Corminboeuf, R. Puchta and P. V. R. Schleyer, *Chem. Rev.*, 2005, **10**, 3842–3888.